Separation and Purification Technology 332 (2024) 125783

Contents lists available at ScienceDirect

Separation and Purification Technology

journal homepage: www.elsevier.com/locate/seppur

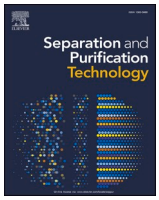

Molecular layer deposition of conjugated microporous polymers (CMPs) thin films for fast molecular sieving

Kai Mi [a], Xingpei Ji [a], Sen Xiong [a,*], Yong Wang [a,b,*]

[a] State Key Laboratory of Materials-Oriented Chemical Engineering, College of Chemical Engineering, Nanjing Tech University, Nanjing 211816, PR China
[b] School of Energy and Environment, Southeast University, Nanjing 210096, Jiangsu, PR China

ARTICLE INFO

Keywords:
Molecular layer deposition
Conjugated microporous polymers
Microporous membrane
Molecular-level design

ABSTRACT

Conjugated microporous polymers (CMPs) have great potential in membrane separation for their intrinsic microporosity and outstanding stability. Unfortunately, most CMPs are insoluble and infusible, thus it is very challenging to prepare CMPs membranes through conventional strategies. Herein, we report the molecular layer deposition (MLD) strategy to synthesize CMP thin films and their outstanding molecular sieving performances as nanofiltration membranes. Thanks to the gas-phase self-limiting reactions between volatile monomers during MLD, defect-free and large-area CMP thin films are deposited on porous substrates. The thickness of the CMP films is precisely tuned by the repeating MLD cycle numbers, and 100 MLD cycles result in a CMP thin film with the thickness of ~ 70 nm. The as-prepared composite membranes with the deposited MLD thin films as the selective layers exhibit superior molecular sieving properties with a permeance up to 134 L $m^{-2}h^{-1}$ bar^{-1}, outperforming other CMP membranes. In addition, the perm-selectivity of CMP membranes can be easily tuned by changing MLD cycle numbers. We further demonstrate that, by optimizing the deposition process including selecting proper precursors, CMP thin films can be successfully MLD-deposited onto temperature-sensitive polymeric substrates with the size as large as 10 cm × 10 cm. This work shows the feasibility and great potential of MLD synthesis of CMP thin films, which opens new avenues not only for the synthesis of CMPs with highly controllable thickness, but also for the preparation of advanced membranes for diverse applications.

1. Introduction

Conjugated microporous polymers (CMPs), which feature permeant microporous structures and π-conjugation backbones, have emerged as novel microporous materials [1]. CMPs have been extensively studied for potential applications in heterogeneous catalysis [2], light emittance [3], energy storage [4], and separations [5]. Thanks to the advantages of CMPs, such as microporous structures, uniform pore size distribution, and high chemical and thermal stabilities [6], they are particularly suitable for usage in advanced membranes for molecular separations. Tremendous efforts have been made to develop CMP-based membranes for organic solvent nanofiltration (OSN) [7], ion sieving [8], and gas separation [9]. However, most CMPs are insoluble and infusible, and it is very challenging for pre-formed CMPs to directly prepare membranes like ordinary membrane-forming hydrocarbon polymers.

Alternatively, researchers turned to use *in-situ* synthesis strategies to fabricate CMP membranes. Zhang *et al.* fabricated imine-linked CMP membranes *in situ* on modified polyacrylonitrile (PAN) substrates through catalysis diffusion-controlled interfacial polymerization [10]. Owing to the strong reactions between monomers, the CMP thin films were formed on PAN substrates within 10 min, and the resulting membranes showed attractive nanofiltration performance. Tsotsalas *et al.* fabricated CMP membranes through layer-by-layer deposition [9]. To maintain the integrity of the obtained CMP thin films, sacrificial metal–organic framework (MOF) layers were used. The monomers were introduced onto the MOF layers to synthesize intact CMP thin films. Finally, the CMP thin films were transferred to porous supports to obtain composite CMP membranes, which exhibited distinguished separation performance towards gas molecules with smaller kinetic diameters. Tang *et al.* used electrochemical active monomers to synthesize CMP thin films through the electropolymerization method [11]. After polymerization, a polymethyl methacrylate (PMMA) protective layer was spin-coated onto the CMP thin film, then the CMP thin film was peeled off from the substrates and transferred onto porous supports. Thus-

* Corresponding authors at: State Key Laboratory of Materials-Oriented Chemical Engineering, College of Chemical Engineering, Nanjing Tech University, Nanjing 211816, PR China (Y. Wang).
E-mail addresses: xiongsenhg@njtech.edu.cn (S. Xiong), yongwang@seu.edu.cn (Y. Wang).

https://doi.org/10.1016/j.seppur.2023.125783
Received 20 September 2023; Received in revised form 17 November 2023; Accepted 17 November 2023
Available online 19 November 2023

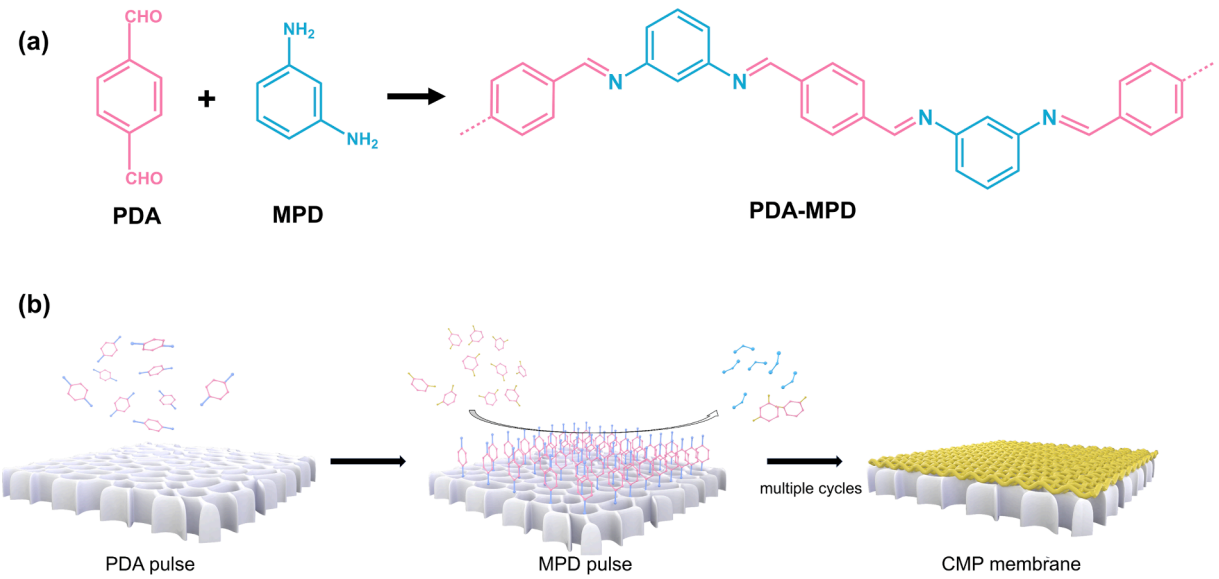

Fig. 1. (a) Synthesis of CMP through the condensation polymerization of the aldehyde monomer of PDA and the amine monomer of MPD. (b) Schematic illustration of the growth of CMP membranes.

prepared CMP composite membranes exhibited an OSN performance with a molecular weight cut off (MWCO) of 800 Da and a methanol permeance of 32 L $m^{-2}h^{-1}$ bar^{-1}. The same group also prepared CMP membranes through surface-initiated polymerization [12]. Silicon wafers were modified with bromobenzene and used as substrates to grow CMP thin films. After 72 h of reaction, CMP thin films with a thickness of ~ 42 nm were grown on the substrates. The CMP thin films were transferred to porous supports to form composite membranes, which showed high permeance towards both nonpolar hexane and polar methanol. However, the uncontrollable CMP thickness, requirements on specific monomers, troublesome transferring steps, and long reaction times greatly limit the large-scale preparation and practical application of CMP-based membranes.

Molecular layer deposition (MLD) is a vapor-phase, surface-confined thin film deposition technique. The working principle of MLD is based on the sequential vaporization of precursors and self-limiting reactions between gaseous precursors [13], thus the deposition layers are grown in the layer-by-layer mode. The major advantages of MLD to fabricate separation membranes are the molecular-level thickness control, and high uniformity and conformality of obtained layers deposited on almost any substrates [14]. This technique has been demonstrated as a powerful tool to synthesize functional materials, including polymers [15,16], MOFs [17,18], and hybrid organic–inorganic materials [19,20] on various substrates. Because the separation performance is largely determined by the thickness and surface chemistry of the separation layer of a membrane, MLD can be used to prepare high-performance membranes by simply changing their thickness as well as surface characteristics. We previously performed polyimide (PI) MLD on polyethersulfone (PES) membranes to enhance the separation performance [21]. After depositing uniform and conformal PI layers onto PES membranes, the pore size of modified membranes was finely tuned and the retention towards 23-nm nanospheres increased from zero to ~ 60%. George *et al.* used trimesoyl chloride and *m*-phenylenediamine as precursors to directly deposit aromatic polyamide (PA) layers onto commercial nanofiltration membranes [22]. With the increasing MLD cycle numbers, the salt rejection of the nanofiltration membranes was improved and the water permeance was correspondingly decreased, demonstrating the capability of MLD to finely tune membrane performance.

In the MLD synthesis of PA and PI, the polymers are formed following the mechanism of polycondensation between two reactive monomers/precursors with the elimination of small molecules. This is very similar to the formation of CMPs. However, as far as we know, MLD has not been explored to synthesize CMPs. In this work, we try to directly synthesize CMPs on porous substrates by MLD to prepare composite membranes with the MLD-deposited CMP thin film as the selective layer. In MLD, the precursors should be easy to volatilize and react with each other. However, the frequently used monomers for CMPs typically possess rigid aromatic rings and complex steric structures, which have low volatility and high steric hindrance that are adverse to MLD processes. To solve this problem, terephthalaldehyde (PDA) and *m*-phenylenediamine (MPD) (Fig. 1**a**), which are relatively volatile, are chosen as precursors to directly deposit CMP on porous substrates (Fig. 1**b**). By selecting suitable precursors, the reaction temperature can be lowered to 100 °C, which significantly expands the choice of substrates. Because of the molecular-level thickness control, thus-prepared CMP membranes show superior permeability and selectivity in molecular separations.

2. Experimental sections

2.1. Materials

With regard to the precursors applied in MLD, PDA (>99%) and MPD (>99%) were purchased from Aladdin (Shanghai, China) and used as received. For different organic dyes used in filtration processes, Congo Red (CR, >99%), Acid Fuchsin (AF, >99%), and Methyl Orange (MO, >99%) were supplied by Tianjin Institute of Chemical Reagent (Tianjin, China). Methyl Blue (MB, >99%), Alcian Blue (AB, >99%), Eriochrome Black T (EBT, >99%), and Brilliant Blue G (BBG, >99%) were provided by Aladdin (Shanghai, China). Rhodamine B (RhB, >99%) was procured from Sigma (Shanghai, China) and Evans Blue (EB, >99%) was acquired from Solarbio (Beijing, China). All dyes were used without further purification. High-purity nitrogen (>99%) was provided by Air Liquide (Suzhou, China) and served as both purge and carrier gases in MLD processes. Si wafers were purchased from Seyang Electronics (Wuxi, China), and anodized aluminum oxide (AAO) disks (disk diameter = 2.5 cm, pore size = 20 nm) were brought from Whatman (Maidstone, England). Poly (vinylidene fluoride) (PVDF) membranes with a pore size of 0.22 μm were purchased from Millipore (Billerica, USA), polytetrafluoroethylene (PTFE) with a pore size of 0.45 μm, and polyamide (PA) with a pore size of 0.1 μm were bought from Delvstlab (Zhejiang, China) and Yibo (Zhejiang, China) filter equipment, respectively. All these

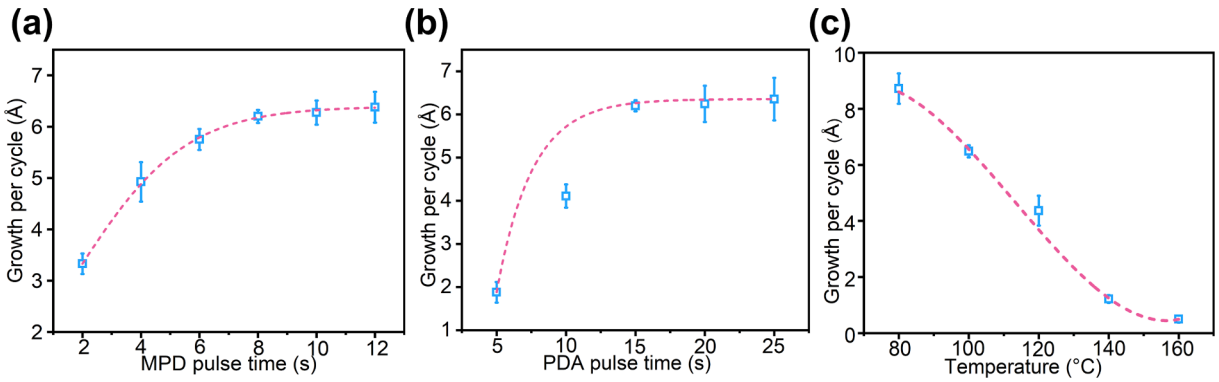

Fig. 2. MLD growth behavior of the CMP thin films on silicon: (a) The influence of MPD and (b) PDA pulse time on GPC. (c) the effect of deposition temperature on GPC.

porous supports were used as substrates.

2.2. Molecular layer deposition processes

The deposition of CMP was conducted in a hot-wall ALD apparatus (Savannah S100, Cambridge NanoTech, USA). During the deposition, a vacuum pump was connected to the reaction chamber to control the background pressure to 1 Torr. Before deposition, PDA and MPD were separately heated to 120 °C and 90 °C to provide sufficient vaporized molecules for deposition, while nitrogen was used as the carrier gas with a flow of 50 sccm. To study the growth behaviors, CMP thin films were first deposited on 2 cm × 2 cm Si substrates at different temperatures, precursor pulse times, and deposition cycles.

For the fabrication of CMP membranes, the MLD process was optimized to obtain dense membranes with appropriate thickness. Prior to deposition, the reaction chamber was heated to 100 °C to ensure an appropriate growth rate. In a standard MLD cycle, the PDA vapor was introduced into the reaction chamber for 15 s, followed by 30 s of nitrogen purge to clean the chamber. Then, the MPD vapor was pulsed for 8 s to react with PDA and formed one molecular layer of CMP. Finally, another nitrogen purge step was followed to clean the reaction chamber again and completed one deposition cycle. The CMP membranes with various thicknesses were prepared by changing deposition cycles and used for further characterization and filtration tests.

2.3. Characterization

Scanning electron microscopy (SEM, S-4800, Hitachi, Japan) was used to study the morphology and thickness of deposited CMP membranes. All samples prepared for SEM were sputter-coated with a thin layer of gold to eliminate the charging effect. Energy dispersive X-ray spectroscopy (EDX, s-4800, Horiba, Japan) was used to analyze the element distribution of the samples. The surface roughness of the deposited layer was observed by atomic force microscopy (AFM, XE-100, Park Systems, South Korea). The water contact angles (WCAs) were used to reveal the hydrophilicity of CMP membranes by a contact angle goniometer (Dropmeter A100, Maist, China). The thicknesses of CMP thin films deposited on Si wafers were determined using a spectroscopic ellipsometer (Complete EASEM-2000U, J. A. Woollam, USA) at an incidence angle of 70° with a wavelength in the range of 200–1000 nm. To investigate the chemical composition of the CMP, Fourier transform infrared (FTIR) spectrometer (Nicolet 8700 spectrometer, Thermo Fisher Scientific, USA) was used in attenuated total reflection (ATR) mode. The thermal stability of the as-deposited CMP membranes was studied utilizing a thermal gravimetric analyzer (TGA, STA 409PC, Netzsch, Germany) under a nitrogen atmosphere with a heating rate of 10 °C·min^{-1}. The nitrogen adsorption isotherm of CMP was recorded on a surface area and porosimetry system (ASAP2460, Micromeritics, USA). The surface area and microporosity of CMP were calculated by using Brunauer-Emmet-Teller (BET) equation and the pore size distribution was determined by utilizing the non-local density functional theory (NLDFT). To prepare the samples for nitrogen adsorption, CMP thin films with micrometer-meter thickness were synthesized using the chemical vapor deposition method at the same temperature adopted in MLD processes. In order to determine the electrical properties of CMP membranes, an electrokinetic analyzer (Surpass 3, Anton Paar, Austria) was used to test the membranes in a 1 mmol/L KCl electrolyte with a pH range from 3 to 10.

2.4. Filtration tests

Nanofiltration tests of CMP membranes prepared by MLD were conducted in a lab-scale dead-end filtration cell driven by nitrogen. The effective area for testing was 0.9 × 10^{-4} m^2 and the testing pressure was 0.5 bar, respectively. The membranes were pre-pressed for at least 30 min before any testing to obtain steady results. A dye solution with a concentration of 25 ppm was utilized as the feed. The molecular weight cut-off (MWCO) was determined through a PEG retention test with various molecular weights (200, 400, 1000, and 2000 Da). The permeance flux (J) was calculated using the following equation:

$$J = \frac{V}{A \times t} \tag{1}$$

where V (L) is the volume of permeate, A (m^2) is the effective membrane area and t (h) is the time required for permeation, respectively. Permeance (P) was normalized to the applied pressure (Δp), and it was calculated as follows:

$$P = \frac{V}{A \times T \times \Delta P} \tag{2}$$

Different dye concentrations were analyzed by a UV–vis absorption spectrometer (NanoDrop 2000c, Thermo Fisher Scientific, USA). The PEG solution concentrations were determined using gel permeation chromatography (GPC, Waters 1515). The rejection (R) of CMP membranes for different dye molecules is obtained using the following equation:

$$R = \left(1 - \frac{c_p}{c_f}\right) \times 100 \tag{3}$$

where C_p (mg·L^{-1}) and C_f (mg·L^{-1}) represent the dye concentration in the permeate and the feed solution, respectively. All filtration tests were repeated at least three times.

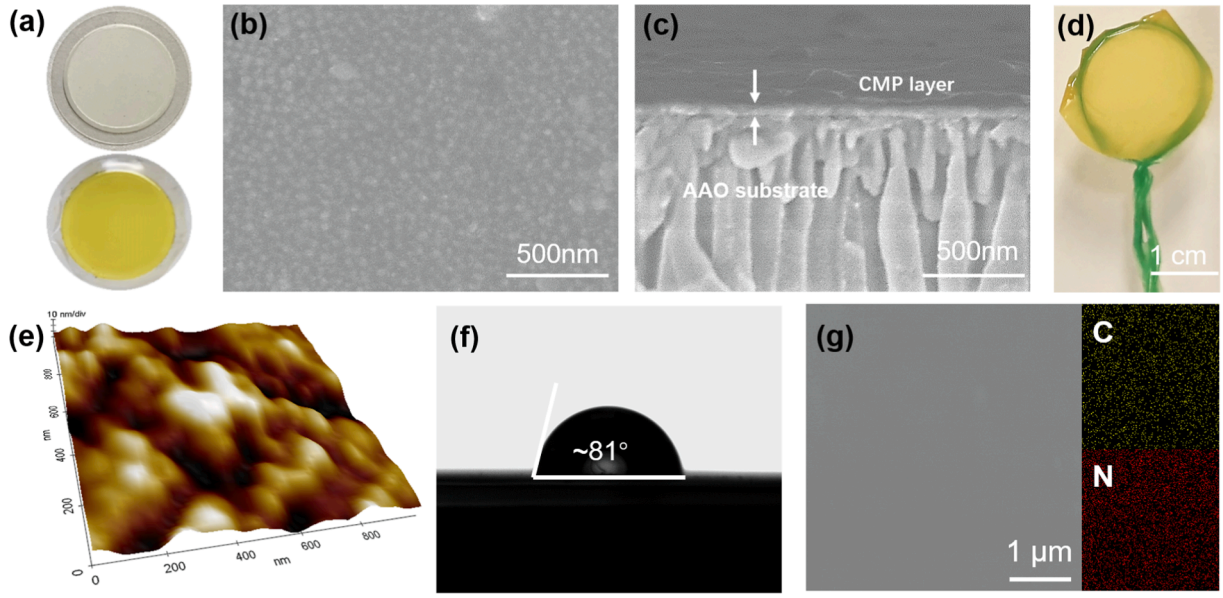

Fig. 3. (a) Photographs of the AAO support (up) and CMP-100 membrane. (b) Surface and (c) cross-section SEM images of CMP-100 membrane. (d) Photograph of the s-CMP-100 layer on a metal lasso. (e) AFM image of the CMP-100 membrane. (f) WCA of the CMP-100 membrane. (g) Surface elemental mapping of the CMP-100 membrane.

3. Results and discussion

3.1. Growth behaviours of CMP in MLD processes

In this work, PDA and MPD are selected as MLD precursors for two reasons. Firstly, both precursors can be sublimated at a relatively low temperature, which significantly facilitates the low-temperature deposition processes. Secondly, smaller molecular size can avoid steric hindrance and accelerate the reaction between two precursors [23]. For the MLD process, the precursor dosage and reaction temperature both had decisive impacts on the quality of deposition layers. Understanding the parameters involved is crucial for the success of MLD in various applications. Thus, the precursor dosage and reaction temperature were carefully investigated to obtain optimized deposition conditions for CMP membrane formation.

To study the impact of precursor pulse on the film growth rate, the pulse time for each precursor was intentionally extended to ensure an optimal layer-by-layer deposition process. As depicted in Fig. 2a, the pulse time for PDA remained constant at 15 s to isolate the investigation of the MPD pulse time. As the MPD pulse time was extended from 2 s to 8 s, the growth per cycle (GPC) of the CMP thin film increased from 3.3 Å to 6.2 Å. Nevertheless, further increasing the MPD pulse time to 12 s did not result in a significant increase in GPC, hinting the saturation adsorption on the substrate [24]. Such a phenomenon also occurred in the study of the PDA pulse time. With a fixed pulse time of MPD (8 s), the GPC increased from ~ 2 Å to ~ 6.3 Å with the PDA pulse time extended from 5 s to 15 s, while the GPC value did not show significant changes even the pulse time was higher than 20 s (Fig. 2**b**). These results indicate that the self-limiting type growth can be achieved with a pulse time of 15 s for PDA and 8 s for MPD, respectively. Consequently, the optimized deposition sequence was determined to be 15 s PDA pulse, 30 s N_2 purge, 8 s MPD pulse and another 30 s N_2 purge in this work.

In MLD, temperature is another decisive factor in the deposition processes. Insufficient deposition temperature may lead to condensation of precursors, and too high temperature may cause desorption or precursor decomposition. Both situations will undermine the quality of deposited layers [25]. Hence, the influence of temperature must be taken into consideration during the deposition process. Based on the aforementioned deposition sequence, the effect of deposition temperature was studied. As shown in Fig. 2**c**, the growth rate decreased from 8.7 Å to 0.5 Å as the deposition temperature increased from 80 °C to 160 °C, which was a typical trend in most MLD or atomic layer deposition (ALD) systems [16]. Considering the fact that a low growth rate was unfavorable in the formation of defect-free separation membranes, 100 °C was selected for the deposition of CMP membrane, which contributed to a medium GPC value of 6.4 Å. Moreover, it can be expected that such a low deposition temperature will expand the MLD of CMP thin films on different substrates, especially on the temperature-sensitive polymeric substrates [26]. The relationship between film thickness and MLD deposition cycles was shown in **Fig. S1**. The growth mode of the CMP thin film obeys the typical layer-by-layer growth mode in MLD, as the thickness of the CMP thin film increases linearly with the number of cycles.

3.2. Fabrication and characterization of CMP membranes

In the investigation of MLD processes on porous substrates, AAO disks with a nominal pore size of 20 nm were selected as the support layers. The CMP thin film was directly synthesized on porous AAO substrates to generate composite membranes (denoted as CMP-*x* membranes, the × represents the number of MLD cycles) by the sequential pulse of PDA and MPD. The structure and corresponding thickness of membranes played a crucial role in determining the separation performance, therefore, the structural features of CMP membranes were thoroughly investigated in this work. Fig. 3**a** exhibits the digital photograph of the CMP-100 membrane. MLD resulted in a luminous yellow-colored CMP thin film covering the original milky AAO substrate, indicating successful deposition of the CMP thin film. Thus-synthesized CMP membranes were further characterized by SEM. At low deposition cycles (25 cycles), the deposition was at the nucleation stage, thus only discrete particles were found on AAO substrates (**Fig. S2**). With the increase of deposition numbers, deposited particles gradually proliferated into a defect-free layer. As shown in Fig. 3**b**,100 cycles of deposition were enough to generate dense CMP thin films without any visible defects, while the AAO pores could still be observed due to the ultrathin nature of the deposited layer [27]. The corresponding cross-sectional SEM image evidenced a continuous CMP thin film on the AAO substrate, and the top thickness of the selective layer was ~ 70 nm (Fig. 3**c**). Also, the CMP-150 membrane exhibited a compact selective layer with a thickness of ~ 110 nm (**Fig. S3**). Besides,

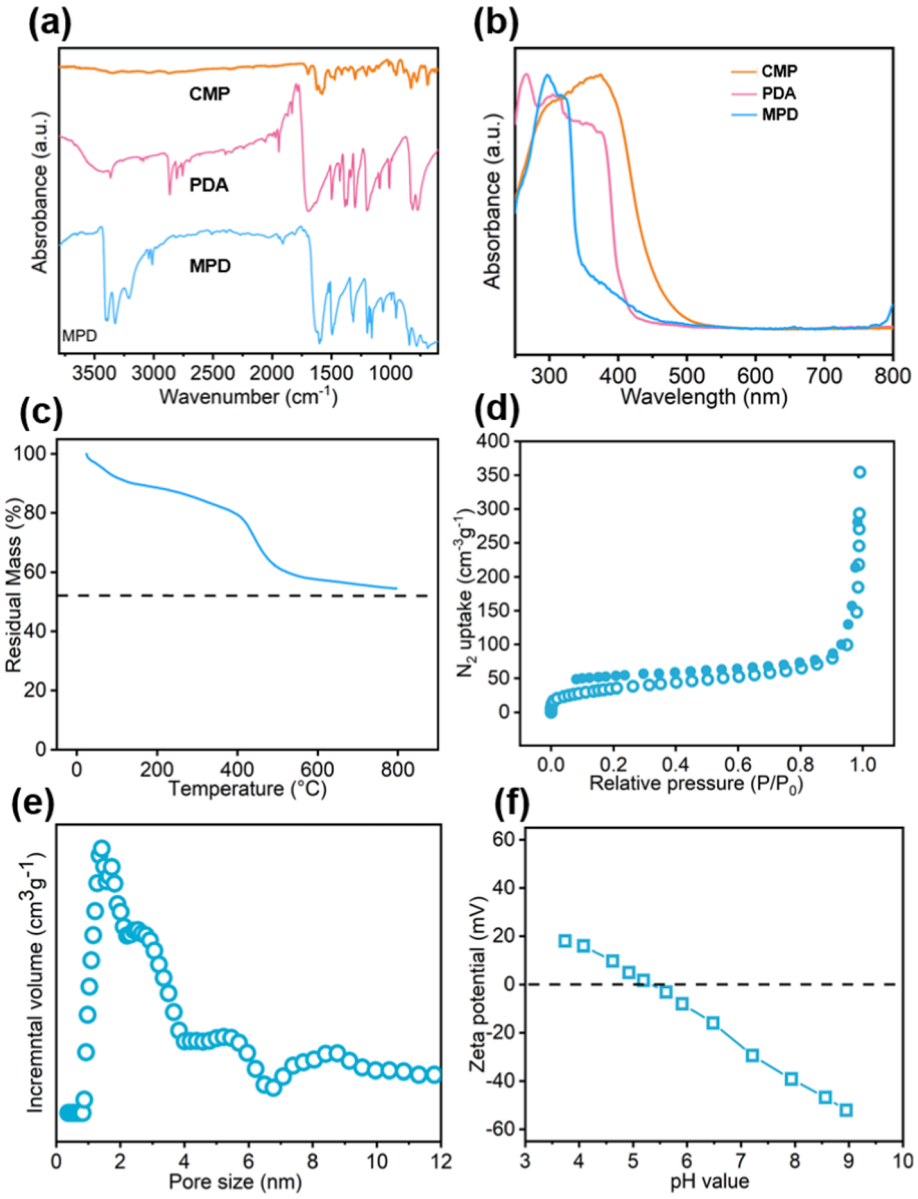

Fig. 4. Chemical and structure characterizations of the CMP-150 membrane. (a) FTIR spectra of the monomers and the membrane. (b) Solid-state UV–vis spectra of the monomers and the membrane. (c) Thermogravimetry analysis of the CMP membrane. (d) Nitrogen sorption isotherm and (e) Pore size distribution of self-supporting CMP films. (f) Zeta potential of the CMP-150 membrane.

a reduction in pore size was observed on the backside of the AAO substrate with a pore size of 100 nm, as shown in Fig. S4. Considering that the precursor vapor diffused to the surface as well as the backside of the AAO substrate simultaneously during MLD, it can be concluded smaller pores on the AAO substrate (20 nm) appears to facilitate the formation of conformal CMP layers. To analyze the structure of the CMP thin film, the CMP-100 membrane was immersed in a 1 mol·L^{-1} sodium hydroxide solution to dissolve the AAO substrate, producing a self-supporting CMP thin film (denoted as s-CMP-100). Optical microscopy disclosed that no cracks and ruptures were present in the s-CMP-100 (Fig. S5). Then the s-CMP-100 was transferred to a metal lasso and it was able to cover the metal lasso completely, implying the outstanding mechanical stability of the MLD-deposited CMP thin films (Fig. 3**d**). CMP-100 membranes prepared by MLD exhibited a smooth surface as the value of surface roughness determined by AFM was as low as 5.35 nm (Fig. 3**e**). Considering that AAO substrates inherently possesses a porous surface, these results further demonstrated the capability of MLD to create highly conformal layers on complex substrates. Additionally, WCA measurement revealed that the CMP had a slightly hydrophilic surface with a contact angle of ~ 81° (Fig. 3**f**). The chemical composition of CMP-100 membranes was further verified by EDX. As expected, the CMP membrane exhibited a uniform element distribution of C and N as a result of the unparalleled diffusion capability of gas-phase precursor molecules during MLD (Fig. 3**g**) [28]. All these results demonstrate that MLD can construct conformal, controllable, and robust CMP thin films onto porous substrates.

CMPs are typically insoluble in organic solvents due to their rigid backbone, which also makes them difficult to be processed into membranes by *ex situ* methods. In this work, two bifunctional precursors were chosen for MLD processes to fabricate CMP membranes. Benefiting from their smaller steric hindrances, the Schiff base reaction can proceed without the use of catalysts in the gas phase. The chemical composition of the as-deposited CMP membranes was first confirmed by ATR-FTIR spectroscopy. As illustrated in Fig. 4**a**, the —NH_2 bonds of MPD in the 3200–3300 cm^{-1} vanished after deposition. Similarly, the peaks between 2720–2870 cm^{-1} originating from —CHO groups in PDA also

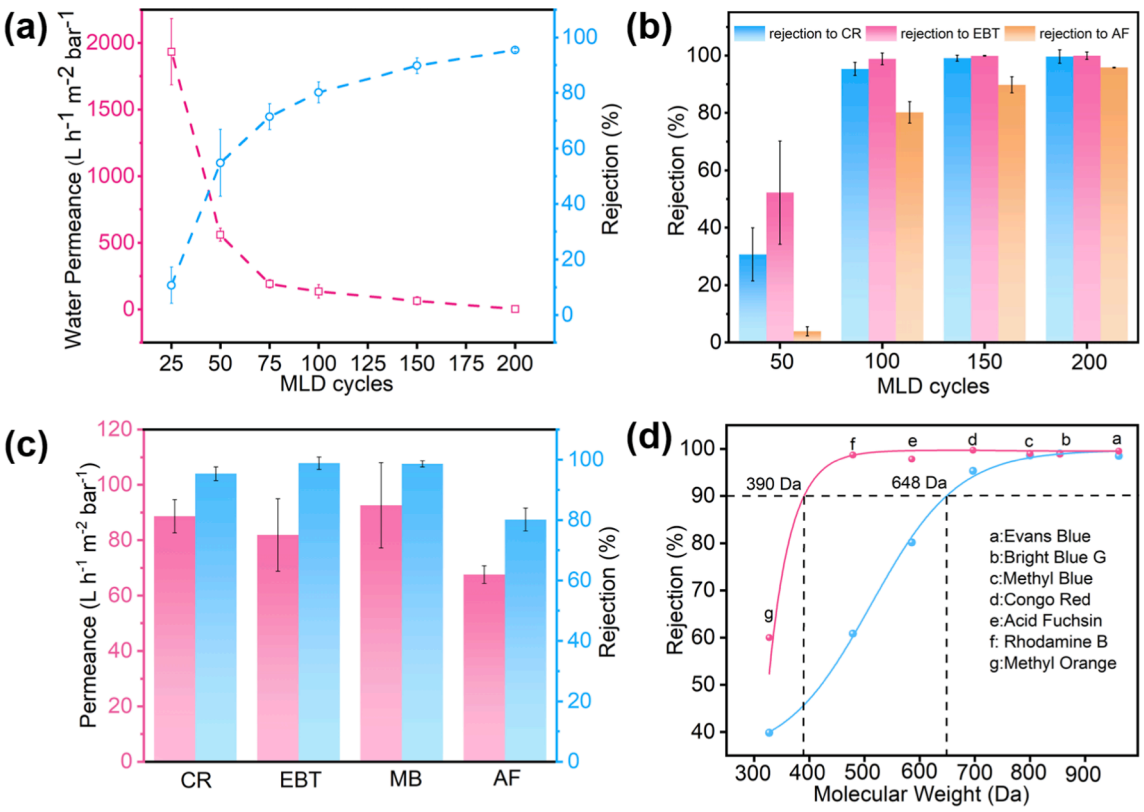

Fig. 5. The molecular sieving capability of CMP membranes. (a) Effects of MLD cycles on water permeance and AF rejection. (b) Relations between deposition cycles and rejections toward different dye molecules. (c) Rejection and permeance of the CMP-100 membrane toward different negatively charged dyes. (d) MWCOs of the CMP-100 and CMP-150 membrane.

disappeared after deposition. Moreover, a new peak belonging to the —C═N— band appeared at 1621 cm^{-1} in the spectra of CMP membranes, which was consistent with the XPS result (Fig. S6) and confirmed the successful condensation between PDA and MPD. Furthermore, the normalized UV–vis spectrum of the CMP membrane exhibited a broader absorption peak (Fig. 4**b**), and exhibited a red shift of maximum absorption peak to 375 nm, suggesting a prolonged conjunction length from the repeated —C═N— bond in the backbones [29]. TGA was conducted in a nitrogen atmosphere. As shown in Fig. 4**c**, the CMP could maintain 54.5% weight even at 800 °C. Two main weight loss stages were observed in the TGA curve, which could be ascribed to the desorption of water (from 50 °C to 120 °C) and the decomposition of the imide CMP backbone (from 420 °C to 480 °C), respectively (Fig. S7). This result demonstrated the success of the MLD process to synthesize CMP thin films and their outstanding thermal stability. The porosity of the CMP thin film was characterized by the N_2 adsorption–desorption results (Fig. 4**d**). A significant increase in adsorption capacity was observed in the ultralow relative pressure region ($P/P_0 < 0.05$), which indicated the existence of abundant micropores [30]. According to the adsorption isotherm, the surface area of the PDA-MPD film was 128 $m^2 \cdot g^{-1}$. The pore size distribution of the self-supporting CMP thin film was evaluated using the NLDFT method. As shown in Fig. 4**e**, the CMP membrane exhibited a narrow distribution of pore apertures centering at 1.35 nm. The zeta potential characterization demonstrated that the CMP exhibited a strongly negatively charged surface in a wide pH range (Fig. 4**f**), which is expected to be in favor of improving the molecular sieving capability to negatively charged molecules [31]. The negative surface charge should be attributed to the electronegative carbonyl oxygen stemming from the unreacted aldehyde groups of PDA [32]. Moreover, the amorphous structure of CMP was proved by XRD. The XRD pattern of the self-supporting CMP films only showed a wide and elongated absorption peak, which confirmed that the MLD-deposited CMP in this work was amorphous. (Fig. S8).

3.3. *Molecular sieving capability of CMP membranes*

The molecular sieving capability of CMP membranes prepared by MLD with different cycles was investigated to reveal the relationship between membrane thickness and nanofiltration performance, and the tunability of membrane thickness of MLD provides a valuable tool [22]. In general, membranes that exhibit a fast permeation are generally less selective, and *vice versa*. Thus, the balance between membrane thickness and structural integrity should be achieved to reconcile permeability and selectivity [33]. In order to understand the relationship between membrane structure and separation performance, the rejections of Acid Fuchsin (AF) and corresponding pure water permeance (PWP) of CMP membranes were rated as a function of deposition cycles. As shown in Fig. 5**a**, with the deposition cycles of CMP membranes varied from 25 to 200, the rejection of AF was progressively increased from 10.7% to 95.5%, whereas the PWP was decreased from 1933.4 to 2.5 L/h m^{-2} bar^{-1}. With low deposition cycles, a nucleation period was essential for CMP to cover the porous surface of AAO substrates [34]. During this period, the pore on the substrates could not be completely blocked, thus leading to a low rejection. As MLD cycles increased to 100, deposited nanoparticles gradually proliferated into a defect-free CMP film with a thickness of ~ 70 nm, exhibiting a rejection of 80.2% toward AF and the PWP remained at a relatively high level of 134.8 L/h m^{-2} bar^{-1}. The thickness of the CMP membrane was linearly enlarged to 110 nm with 150 cycles of MLD, and a rejection of 90% with a PWP of 64.0 L/h m^{-2} bar^{-1} was achieved. That is, the nanofiltration properties of our CMP membranes can be precisely controlled by simply changing the number of MLD cycles.

The molecular sieving capability of CMP membranes was further evaluated by using other dye molecules, namely Congo Red (CR) and

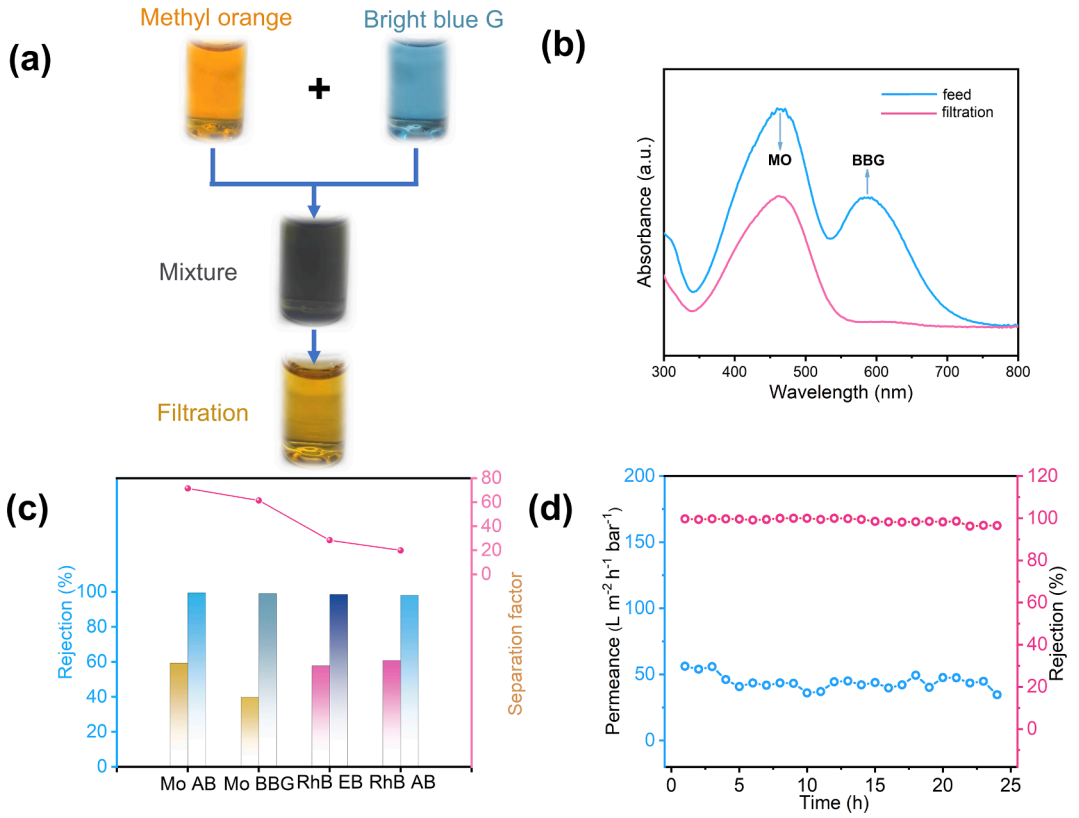

Fig. 6. (a) Photographs of the dye solution before and after separation. (b) UV spectra of dye mixture before and after filtration. (c) Separation performances of the CMP-100 membrane toward mixtures of dyes. (d) Long-term stability of the CMP-150 membrane in a 24 h filtration testing.

Eriochrome Black T (EBT). Their dimensions and corresponding molecular weights were summarized in **Table S1**. As shown in Fig. 5**b**, CMP membranes prepared with higher deposition cycles showed an increasing trend in rejection. To be specific, as the deposition cycles were increased from 50 to 200, the rejection of CMP membranes towards CR and EBT was increased from 30.7% to 99.6% and from 52.2% to 99.9%, respectively. By comparing all the rejection data of the CMP membranes, it could be observed that the CMP membranes showed lower rejections towards dyes with smaller molecule weights. In general, CMP membranes prepared by MLD exhibited decent rejections toward various dyes, which could be attributed to both size sieving and electrostatic repulsion effects between the negatively charged dye molecules and CMP membranes [35].

To fully understand the mechanism of dye removing processes, the effect of adsorption must be excluded [36]. We first checked the concentration of dye molecules in retentate. As confirmed by UV–vis spectra (**Fig. S10**), the concentration of retentate was significantly increased compared to that of the corresponding feed solution, indicating of the negligible effect of adsorption. Additionally, long static adsorption results further proved the absence of adsorption. The UV–vis spectra of various dye molecules remained unchanged after static adsorption for 24 h (**Fig. S11**). Meanwhile, the CMP membrane could keep its shape after being immersed in water for at least 3 weeks, which confirmed the CMP membrane was stable to be used in aqueous environments (**Fig. S12**).

Considering the balance between membrane thickness and structural integrity, we tested CMP-100 membranes for further investigation. CMP was expected to adequately reject molecules larger than its intrinsic pore size. As shown in Fig. 5**c**, the CMP-100 membrane could reject 98.6%, 95.3%, 99.0%, and 80.2% of MB, CR, EBT, and AF, respectively. Meanwhile, the permeance for all dye solutions was higher than 70 $L{\cdot}h^{-1}{\cdot}m^{-2}{\cdot}bar^{-1}$. It should be noted that permeances of dye solutions were essentially lower than that of PWP due to the formation of a dye-cake layer during filtration of the former [31].

To highlight the ability of MLD to precisely tune the nanofiltration properties of membranes, the effect of changing MLD cycles on the MWCO of CMP membranes was investigated. As shown in Fig. 5**d**, the CMP-100 membrane and CMP-150 membrane generate a MWCO of 647 Da and 389 Da, respectively. The high rejection can be mainly attributed to two aspects, size exclusion and electrostatic repulsion effects between the charged dye molecules and CMP membranes. Specifically, the high rejection of CMP-150 toward AF and RhB was mainly attributed to the difference in mass transfer resistance of a thicker selective layer, as CMP-100 only exhibited a rejection rate of 80.2% and 60.8% toward AF and RhB, respectively. Therefore, it can be concluded that the feature of MLD in finely tuning the thickness of the deposited CMP films makes it easier to fabricate membranes with adjustable separation properties according to the needs of actual separation systems. Besides, the MWCO of the CMP-150 membrane determined through the rejection of neutral poly (ethylene glycol) (PEG) is 690 Da (**Fig. S13**). This MWCO value is larger than that determined by using dyes as the probing molecules, which is because the rejection of neutral PEG is solely based size exclusion while static repulsion also plays a significant role in the rejection of charged dye molecules in addition to size exclusion.

The nanofiltration performance of CMP membranes toward the solution of mixed dyes was tested to evaluate their differentiated molecule sieving capability. A mixture of Methyl Orange (MO) and Brilliant Blue G (BBG) was employed as the feed solution. As shown in Fig. 6**a**, the mixture exhibited a light black colour derived from MO and BBG, whereas the permeate only showed an orange colour originating from MO after filtration by the CMP-100 membrane, indicating BBG molecules were retained. This was further demonstrated by UV–vis spectra (Fig. 6**b**). The characteristic peak at 586 nm which originated from BBG disappeared, while that of MO at 462 nm still remained. Specifically, the CMP-100 membrane efficiently rejected 96% BBG, while only 39% MO was rejected. Moreover, the CMP-100 membranes showed the ability to

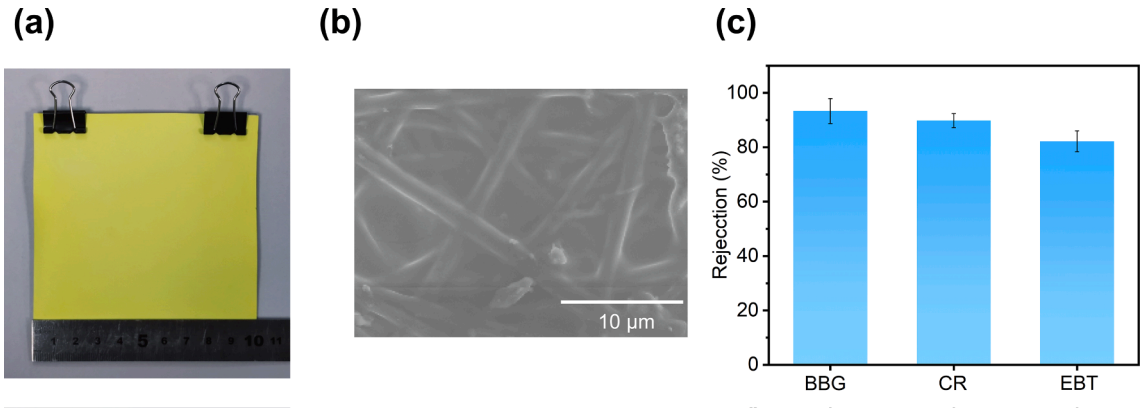

Fig. 7. (a) The photograph of a large-area CMP membrane (10 cm × 10 cm) deposited on PA substrate. (b) SEM image of the large-area CMP membrane. (c) Separation performances of the large-area CMP membrane toward various kinds of dye molecules.

separate various dye mixtures by using the dimensional differences of the dye molecules (Fig. 6**c and S9**), and the separation factor was high up to 71. To investigate the long-term stability of CMP membranes, a 24 h continuous filtration test was conducted. As shown in Fig. 6**d**, the CMP-150 membrane displayed negligible decreases in both CR rejection and corresponding permeance. Furthermore, the CMP membranes prepared through MLD with controlled thickness exhibit outstanding molecular sieving capabilities, surpassing the performance of the majority of state-of-art membranes (**Fig. S17** and **Table S2**).

3.4. Preparation of CMP thin films on organic substrates

As previously mentioned, the low deposition temperature made CMPs possible to deposit on polymeric substrates, which is challenging to accomplish by using other synthetic methods. A series of polymeric substrates, including Poly (vinylidene fluoride) (PVDF), polytetrafluoroethylene (PTFE), and polyamide (PA), were subjected to MLD processes. As depicted in **Fig. S14**, all these polymeric substrates showed a luminous yellow colour after MLD for 200 cycles, and the structural integrity of the substrates remained intact due to the low deposition temperature. SEM characterization further revealed the formation of compact, defect-free CMP thin films on these substrates (**Fig. S15**). We further attempted to fabricate large-area CMP membranes on polymeric substrates through MLD. As shown in Fig. 7**a, a 10** cm × 10 cm CMP thin film on the PA substrate was successfully fabricated. Thus-fabricated composite membrane showed a dense CMP thin film covering the polymeric substrate (Fig. 7**b**). The large-area CMP films deposited on organic porous substrates exhibited lower water permeance toward those deposited on AAO substrates. The water permeance of CMP membranes on the nylon substrate with 200 MLD cycles is ~ 4.5·L $m^{-2}h^{-1}$ bar^{-1}, higher than the counterpart deposited on the AAO substrate with the same MLD cycles, which is due to the higher porosity of the PA substrate. However, the porous organic substrates possessing larger pores compared to AAO, thus, a higher number of deposition cycles (200 cycles) is required to form a defect-free CMP layer. That is, it is not possible to increase the permeance of the CMP membranes deposited on PA substrates by lowering down the MLD cycles without sacrifice the selectivity. Moreover, the large-area CMP membrane exhibited a decent rejection toward different dye molecules (Fig. 7**c and S16**), indicating great potential of using MLD to fabricate CMP membranes on a large scale.

4. Conclusion

In summary, MLD is explored for the precise and solvent-free synthesis of CMP thin films on porous substrates to form CMP composite membranes. The large-area deposition of CMP thin films, which is hard to be achieved by other synthetic methods, is realized by MLD and the defect-free, uniform, and conformal CMP thin films are deposited onto different substrates. With the MLD cycles increasing from 25 to 200, the water permanence varied from 1933.4 to 2.5 L/h m^{-2} bar^{-1} and the rejection towards target dye molecules increased from 10.7% to 95.5%. Among all specimens, the CMP-100 membranes exhibit satisfactory water permeance and dye molecule rejection rates. Moreover, the deposition temperature is lowered to 100 °C by selecting proper precursors, which expands the applications of CMP deposition to temperature-sensitive substrates. As a result, the CMP thin films are successfully deposited onto different polymeric substrates and the size can be up to 10 cm × 10 cm. This method offers a new approach to the preparation of high-performance nanofiltration membranes based on CMPs, which will further expand the applications of high-performance nanofiltration membranes in industries.

CRediT authorship contribution statement

Kai Mi: Conceptualization, Data curation, Methodology, Writing – original draft. **Xingpei Ji:** Formal analysis, Methodology, Validation. **Sen Xiong:** Data curation, Funding acquisition, Supervision, Validation, Writing – review & editing. **Yong Wang:** Methodology, Software, Supervision, Writing – review & editing.

Declaration of Competing Interest

The authors declare that they have no known competing financial interests or personal relationships that could have appeared to influence the work reported in this paper.

Acknowledgments

This work was financially supported by the Key Research and Development Program of the Jiangsu Provincial Department of Science and Technology of China (BE2022056-3) and the National Natural Science Foundation of China (21825803).

Appendix A. Supplementary material

Supplementary data to this article can be found online at https://doi.org/10.1016/j.seppur.2023.125783.

References

[1] J.M. Lee, A.I. Cooper, Advances in Conjugated Microporous Polymers, Chem. Rev. 120 (4) (2020) 2171–2214.
[2] L. Chen, Y. Yang, D. Jiang, CMPs as Scaffolds for Constructing Porous Catalytic Frameworks: A Built-in Heterogeneous Catalyst with High Activity and Selectivity

Based on Nanoporous Metalloporphyrin Polymers, J. Am. Chem. Soc. 132 (26) (2010) 9138–9143.
[3] Y. Xu, A. Nagai, D. Jiang, Core-shell conjugated microporous polymers: a new strategy for exploring color-tunable and -controllable light emissions, Chem. Commun. 49 (16) (2013) 1591–1593.
[4] C. Zhang, Y. Qiao, P. Xiong, W. Ma, P. Bai, X. Wang, Q. Li, J. Zhao, Y. Xu, Y. Chen, J.H. Zeng, F. Wang, Y. Xu, J.X. Jiang, Conjugated Microporous Polymers with Tunable Electronic Structure for High-Performance Potassium-Ion Batteries, ACS Nano 13 (1) (2019) 745–754.
[5] Z. Zhou, Z. Li, L.M. Rehman, Z. Lai, Conjugated microporous polymer membranes for chemical separations, Chin. J. Chem. Eng. 45 (2022) 1–14.
[6] A. Hayat, M. Sohail, A. El Jery, K.M. Al-Zaydi, S. Raza, H. Ali, Y. Al-Hadeethi, T. A. Taha, I. Ud Din, M. Ali Khan, M.A. Amin, E. Ghasali, Y. Orooji, Z. Ajmal, M. Zahid Ansari, Recent advances in ground-breaking conjugated microporous polymers-based materials, their synthesis, modification and potential applications, Mater. Today 64 (2023) 180–208.
[7] R. Hardian, K.A. Miller, L. Cseri, S. Roy, J.M. Gayle, R. Vajtai, P.M. Ajayan, G. Szekely, 2D conjugated microporous polymer membranes for organic solvent nanofiltration, Chem. Eng. J. 452 (2023), 139457.
[8] Z. Zhou, D. Guo, D.B. Shinde, L. Cao, Z. Li, X. Li, D. Lu, Z. Lai, Precise Sub-Angstrom Ion Separation Using Conjugated Microporous Polymer Membranes, ACS Nano 15 (7) (2021) 11970–11980.
[9] P. Lindemann, M. Tsotsalas, S. Shishatskiy, V. Abetz, P. Krolla-Sidenstein, C. Azucena, L. Monnereau, A. Beyer, A. Gölzhäuser, V. Mugnaini, H. Gliemann, S. Bräse, C. Wöll, Preparation of Freestanding Conjugated Microporous Polymer Nanomembranes for Gas Separation, Chem. Mater. 26 (24) (2014) 7189–7193.
[10] K. Li, J. Zhu, D. Liu, Y. Zhang, B. Van der Bruggen, Controllable and Rapid Synthesis of Conjugated Microporous Polymer Membranes via Interfacial Polymerization for Ultrafast Molecular Separation, Chem. Mater. 33 (17) (2021) 7047–7056.
[11] X. He, H. Sin, B. Liang, Z.A. Ghazi, A.M. Khattak, N.A. Khan, H.R. Alanagh, L. Li, X. Lu, Z. Tang, Controlling the Selectivity of Conjugated Microporous Polymer Membrane for Efficient Organic Solvent Nanofiltration, Adv. Fun. Mater. 29 (2019) 1900134.
[12] B. Liang, H. Wang, X. Shi, B. Shen, X. He, Z.A. Ghazi, N.A. Khan, H. Sin, A. M. Khattak, L. Li, Z. Tang, Microporous membranes comprising conjugated polymers with rigid backbones enable ultrafast organic-solvent nanofiltration, Nat. Chem. 10 (9) (2018) 961–967.
[13] X. Meng, An overview of molecular layer deposition for organic and organic–inorganic hybrid materials: mechanisms, growth characteristics, and promising applications, J. Mater. Chem. A 5 (35) (2017) 18326–18378.
[14] W. Szmyt, C. Guerra-Nuñez, L. Huber, C. Dransfeld, I. Utke, Atomic Layer Deposition on Porous Substrates: From General Formulation to Fibrous Substrates and Scaling Laws, Chem. Mater. 34 (1) (2021) 203–216.
[15] T. Yoshimura, R. Ebihara, A. Oshima, Polymer wires with quantum dots grown by molecular layer deposition of three source molecules for sensitized photovoltaics, J. Vac. Sci. Technol., A 29 (2011), 051510.
[16] S.E. Atanasov, M.D. Losego, B. Gong, E. Sachet, J.-P. Maria, P.S. Williams, G. N. Parsons, Highly Conductive and Conformal Poly(3,4-ethylenedioxythiophene) (PEDOT) Thin Films via Oxidative Molecular Layer Deposition, Chem. Mater. 26 (11) (2014) 3471–3478.
[17] K.B. Lausund, O. Nilsen, All-gas-phase synthesis of UiO-66 through modulated atomic layer deposition, Nat. Commun. 7 (2016) 13578.
[18] K.B. Lausund, M.S. Olsen, P.-A. Hansen, H. Valen, O. Nilsen, MOF thin films with bi-aromatic linkers grown by molecular layer deposition, J. Mater. Chem. A 8 (5) (2020) 2539–2548.
[19] B. Yoon, D. Seghete, A.S. Cavanagh, S.M. George, Molecular Layer Deposition of Hybrid Organic−Inorganic Alucone Polymer Films Using a Three-Step ABC Reaction Sequence, Chem. Mater. 21 (22) (2009) 5365–5374.
[20] X. Liang, M. Yu, J. Li, Y.B. Jiang, A.W. Weimer, Ultra-thin microporous-mesoporous metal oxide films prepared by molecular layer deposition (MLD), Chem. Commun. 46 (2009) 7140–7142.
[21] T. Sheng, H. Chen, S. Xiong, X. Chen, Y. Wang, Atomic layer deposition of polyimide on microporous polyethersulfone membranes for enhanced and tunable performances, AIChE J. 60 (10) (2014) 3614–3622.
[22] B.C. Welch, O.M. McIntee, T.J. Myers, A.R. Greenberg, V.M. Bright, S.M. George, Molecular layer deposition for the fabrication of desalination membranes with tunable metrics, Desalination 520 (2021), 115334.
[23] S. Xiong, X. Qian, Z. Zhong, Y. Wang, Atomic layer deposition for membrane modification, functionalization and preparation: A review, J. Membr. Sci. 658 (2022), 120740.
[24] A. Philip, S. Vasala, P. Glatzel, M. Karppinen, Atomic/molecular layer deposition of Ni-terephthalate thin films, Dalton Trans. 50 (44) (2021) 16133–16138.
[25] S.M. George, Atomic Layer Deposition: An Overview, Chem. Rev. 110 (1) (2010) 111–131.
[26] S.G. Im, P.J. Yoo, P.T. Hammond, K.K. Gleason, Grafted Conducting Polymer Films for Nano-patterning onto Various Organic and Inorganic Substrates by Oxidative Chemical Vapor Deposition, Adv. Mater. 19 (19) (2007) 2863–2867.
[27] X. Shi, Z. Zhang, C. Yin, X. Zhang, J. Long, Z. Zhang, Y. Wang, Design of Three-Dimensional Covalent Organic Framework Membranes for Fast and Robust Organic Solvent Nanofiltration, Angew. Chem. Int. Ed. 61 (36) (2022) e202207559.
[28] N.E. Richey, C. de Paula, S.F. Bent, Understanding chemical and physical mechanisms in atomic layer deposition, J. Chem. Phys. 152 (4) (2020), 040902.
[29] Z. Liu, M. Song, S. Ju, X. Huang, X. Wang, X. Shi, Y. Zhu, Z. Wang, J. Chen, H. Li, Y. Cheng, L. Xie, J. Liu, W. Huang, Wafer-Scale Ultrathin Two-Dimensional Conjugated Microporous Polymers: Preparation and Application in Heterostructure Devices, ACS Appl. Mater. Interfaces 10 (4) (2018) 4010–4017.
[30] C. Yin, Z. Zhang, Z. Si, X. Shi, Y. Wang, Smart Covalent Organic Frameworks with Intrapore Azobenzene Groups for Light-Gated Ion Transport, Chem. Mater. 34 (20) (2022) 9212–9220.
[31] R. Wang, Y. Zhou, Y. Zhang, J. Xue, J. Caro, H. Wang, Ultrathin Covalent Organic Framework Membranes Prepared by Rapid Electrophoretic Deposition, Adv. Mater. 34 (44) (2022) e2204894.
[32] J. Long, X. Shi, T. Ju, X. Wang, Z. Zhang, Y. Wang, Rapid synthesis of ultrathin covalent organic polymer membranes with subnanometer pores for efficient organic solvent nanofiltration, J. Membr. Sci. 684 (2023), 121880.
[33] C. Yin, Z. Zhang, J. Zhou, Y. Wang, Single-Layered Nanosheets of Covalent Triazine Frameworks (CTFs) by Mild Oxidation for Molecular-Sieving Membranes, ACS Appl. Mater. Interfaces 12 (16) (2020) 18944–18951.
[34] R.L. Puurunen, Surface chemistry of atomic layer deposition: A case study for the trimethylaluminum/water process, J. Appl. Phys. 97 (2005), 121301.
[35] X. Wang, J. Yang, X. Shi, Z. Zhang, C. Yin, Y. Wang, Electrosynthesis of Ionic Covalent Organic Frameworks for Charge-Selective Separation of Molecules, Small 18 (15) (2022) e2107108.
[36] J.L. Fenton, D.W. Burke, D. Qian, M.O. Cruz, W.R. Dichtel, Polycrystalline Covalent Organic Framework Films Act as Adsorbents, Not Membr. J. Am. Chem. Soc. 143 (3) (2021) 1466–1473.